Design Studies for a TPC Readout Plane Using Zigzag Patterns With Multistage GEM Detectors

B. Azmoun, P. Garg, T. K. Hemmick, M. Hohlmann, A. Kiselev, M. L. Purschke, C. Woody, and A. Zhang

***Abstract*— New design studies have been carried out for a readout plane for gas electron multiplier detectors using zigzag patterns that can significantly reduce the readout channel count while preserving excellent spatial resolution for tracking detectors. While zigzag patterns have been used in a number of applications, these studies were designed to investigate the fundamental limits of charge sharing between the electrodes to optimize the spatial resolution and minimize the nonuniformities across the readout plane, while exploring the limits of manufacturing capabilities for producing the readout board. Simulation studies were carried out to optimize the readout electrode structure, and readout boards were produced with similar zigzag designs that were tested in the laboratory using a scanning X-ray source. These studies were aimed at developing a readout board for the new time projection chamber for the sPHENIX experiment at relativistic heavy ion collider, but can readily be used in other applications, including various micropattern gas detectors, such as Micromegas.**

***Index Terms*— Chevron, gas detector, gas electron multiplier (GEM), MPGP, readout, time projection chamber (TPC), zigzag.**

I. Introduction

MODERN day tracking detectors make extensive use of micropattern gas detectors, such as gas electron multipliers (GEMs) [8] and Micromegas [5], which can deliver high-precision spatial coordinates, but the readout of such high-resolution coordinates can require a large number of readout channels, especially in a high-track multiplicity environment where a high degree of spatial segmentation is required. One such application is for a time projection chamber (TPC), which typically has a highly segmented readout plane at the end of its drift volume. A new TPC is currently being designed for the sPHENIX experiment at relativistic heavy ion collider [10] that requires a readout plane with a single-point resolution around 100 μm to measure high-energy particle tracks in heavy ion collisions. Due to possible constraints on the front-end electronics for such applications, these studies were motivated by the need to achieve a good spatial resolution with as few readout channels as reasonably possible.

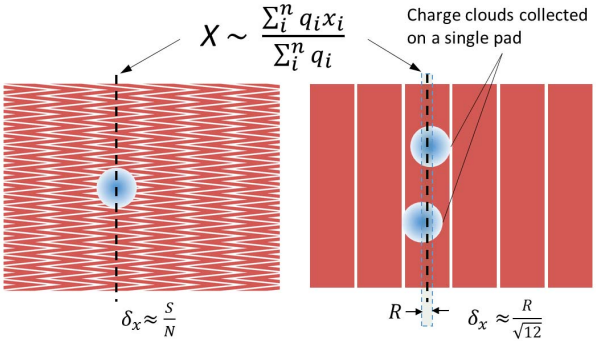

Fig. 1. Sketches of two different readout patterns demonstrate charge sharing and its impact on the centroid calculation and the related position error for a zigzag and rectangular pad geometry. Six channels are shown for each pattern with the same pitch. (The drawings are to scale.)

The so-called zigzag (or chevron) readout patterns have been used for many years to provide high-resolution space points with a minimal number of readout electrodes [1], [4], [6], [7], [11], [13]. This technique utilizes charge sharing to spread the charge from a gas avalanche over a pattern of interleaved electrodes that in principle share the charge proportionally between them depending on the position of the charge cloud. However, in a real implementation of this technique, various physical limitations are encountered that affect the linearity of charge sharing which leads to differential nonlinearities (DNLs, i.e., in this context, a measure of the deviation from a linear response) that can ultimately limit the achievable spatial resolution.

The basis for employing zigzags is shown in Fig. 1. The advantage of utilizing zigzag pads over more standard rectangular pads is that the response of rectangular pads can be strongly influenced by single-pad hits, whose rms error is the standard deviation of a uniform distribution over the region of a pad where charge sharing is not possible (denoted by the width R). This is clear for the particular case where the collected charge cloud is roughly the same size as the pitch of each readout pattern. Hypothetically, a zigzag structure divides the impingent charge in near exact proportion to its center of gravity everywhere along the readout, and therefore, the reconstructed hit position is virtually free of any systematic error stemming from the charge-sharing stage. Therefore, while the response of well-designed zigzags is believed to be mostly governed by secondary factors like

Manuscript received January 6, 2018; revised May 23, 2018; accepted May 31, 2018. Date of publication June 11, 2018; date of current version July 16, 2018. This work was supported by the U.S. Department of Energy under Prime Contract DE-SC0012704.

B. Azmoun, A. Kiselev, M. L. Purschke, C. Woody, and A. Zhang are with the Brookhaven National Laboratory, Upton, NY 11973 USA (e-mail: azmoun@bnl.gov).

P. Garg and T. K. Hemmick are with the Department of Physics and Astronomy, The State University of New York, Stony Brook University, Stony Brook, NY 11794 USA.

M. Hohlmann is with the Florida Institute of Technology, Melbourne, FL 32901 USA.

Color versions of one or more of the figures in this paper are available online at http://ieeexplore.ieee.org.

Digital Object Identifier 10.1109/TNS.2018.2846403

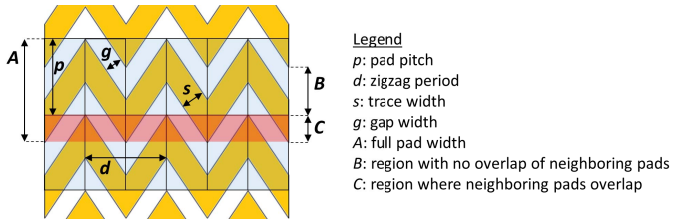

Fig. 2. Sketch of a basic zigzag pattern showing the four defining parameters of the pattern, including the pitch, zigzag period, gap width, and trace width, along with several resultant parameters.

the signal-to-noise (S/N) ratio, similarly sized rectangular pads can be highly susceptible to single-pad hits, which will severely deteriorate the overall resolution. A comparison of the performance of these two readout schemes, for a particular rectangular strip geometry and a less than optimal zigzag pattern, is given in [3]. Additional studies of zigzag or chevron pad structures are provided in the remaining references for completeness.

The purpose of these studies was to investigate the factors which can limit the spatial resolution using zigzag readout patterns by performing Monte Carlo simulations to study these effects in an idealized situation and to understand the fundamental limitations of the readout under certain circumstances. Subsequently, we produced physical readout boards with similar zigzag designs and studied them in the laboratory using a high-precision scanning X-ray source. We report on the results of these simulation studies and on the test results from readout boards produced by two different manufacturers. In particular, we explore the causal link between the physical parameters of the zigzag patterns and the linearity of response from each manufactured board.

II. Results

A. Simulation

The objective of this paper is to optimize the four parameters that define the zigzag pattern in terms of providing linear charge sharing among neighboring pads such that a homogeneous response is observed across the full-readout plane. Fig. 2 illustrates the parametrization used to define the zigzag geometry. A basic zigzag pattern was chosen since this is the simplest arrangement to split charge in proportion to the hit position, while allowing each pad or strip to extend beyond its pitch (typically by a factor of two). Initially, the pad response was studied via a rudimentary simulation, which neglects gas processes and simply allows for the uniform collection of charge onto each pad, governed by the pad geometry alone. The simulated charge cloud is a 2-D Gaussian distribution, whose center is scanned across the zigzag structure, and at each point a charge weighted mean (or centroid) is computed to reconstruct the hit position. The charge on each pad is convoluted with a Gaussian function with a sigma equal to 2% of the average charge collected by the pads to account for a realistic S/N ratio in the system. Some of the results from this simulation are shown in Figs. 3 and 4 for an ideal zigzag pattern featuring 100% pad overlap, a relatively small zigzag period compared to the size of the charge cloud, and a zero-gap width, resulting in 100% conductor coverage on the readout

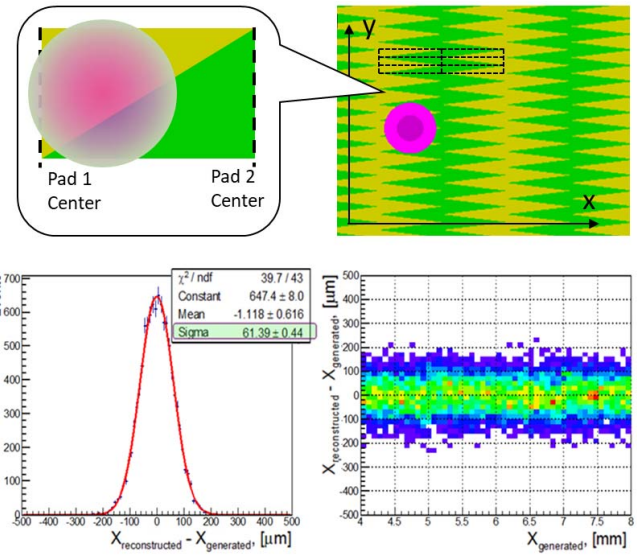

Fig. 3. Sketches of idealized zigzag pads with a zero space gap between them (top). They conceptually reveal the linear relationship between the distributed charge and the hit position. Resultant resolution (~60 μm) for a 2-D Gaussian charge cloud (with $\sigma_x = \sigma_y = 400$ μm) and the pad response for a 2-mm pitch and a 0.5-mm zigzag period (bottom).

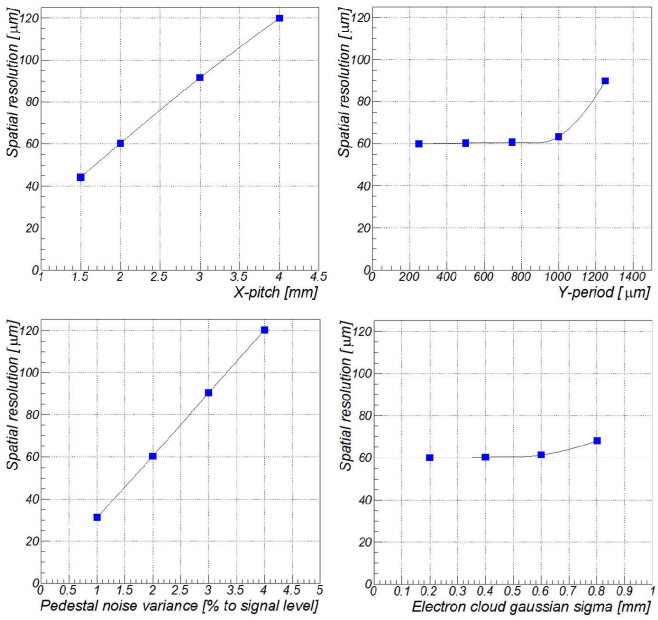

Fig. 4. Simulation results showing the dependence of the position resolution on certain experimental parameters including the zigzag pitch and period (top), and the pedestal noise variance and electron cloud size (bottom). All the plots are generated using the same parameter values as above: 2-mm pitch, 0.5-mm zigzag period, 2-D Gaussian charge cloud (with $\sigma_x = \sigma_y = 400$ μm), and $N/S = 2\%$.

plane. This pattern exhibits a linear response with negligible DNL and a spatial resolution an order magnitude better than what is implied by the physical extent of the pad itself along the position-sensitive coordinate. After studying the effects of varying the zigzag parameters, in addition to the size of the charge cloud, several important attributes of such a linear charge-sharing model were revealed, and are summarized as follows.

- Charge sharing is directly proportional to the hit position as long as the zigzag pitch and period are chosen such that the charge cloud footprint impinges two or three pads, as indicated in Fig. 3. Single-pad hits severely deteriorate the cumulative position resolution (as shown in Fig. 1) and must be avoided. Also, there is a direct correlation between the pitch of the readout and the resultant position resolution, as shown in Fig. 4.
- The zigzag overlap must approach 100%, with minimal strip-to-strip gap width to help ensure that the deposited charge is always collected by more than one pad and the minimal charge collected by any single pad is above a minimum value, as determined by the S/N ratio of the system. A clear linear dependence of the spatial resolution on the noise variance was found, making the S/N a critical factor, as shown in Fig. 4.
- Overstretching the zigzags such that the pad overlap exceeds 100% tends toward a nonlinear response since the collected charge is not necessarily split in proportion to the hit position between the three pads in this geometry [13].
- The zigzag period should be minimized to eliminate a fluctuating response along the zigzag pattern since an overly large period will sample the charge cloud differently along the zigzag structure, as shown in Fig. 4.
- The position resolution is independent of the charge cloud size over a relatively broad range of sizes, assuming primary ionization statistics are sufficiently high. As shown in Fig. 4, the position resolution was maintained for charge clouds as small as 10% of the pitch (taken as the sigma of the charge cloud Gaussian profile divided by the zigzag pitch) and extended to at least four times this value.
- Ideally, the collective response of all fired pads is linearly correlated with the hit position, with a DNL approaching zero at every point along the sensitive coordinate of the readout. For example, it was found that in the limit where the gap width approaches zero and for exactly 100% pad overlap, there are no observable global shifts in the reconstructed hit position over several pitch cycles, as shown in Fig. 3 (bottom right).
- In principle, there are few limiting factors for the achievable position resolution due to the charge-sharing stage of a detector readout when optimized zigzag pads are employed, including practical issues such as S/N ratio and fabrication constraints. (This excludes the hard limits on the position error imposed by primary ionization statistics and transverse diffusion.)
- An optimized pad design avoids corrections for a DNL, which are never 100% efficient and in general depend on the charge cloud footprint size [3]. Specifically, such corrections usually involve applying global offsets to the data, which on average reduce the error, but may not fully eliminate it on an event-by-event basis.

A separate simulation, specific to this detector application, utilizes a finite-element program (ANSYS) to approximate the electric field in the induction gap of a quadruple GEM detector, responsible for carrying individual electrons of the charge cloud to the pad plane. This simulation also employs Garfield++ to take into account gas processes, including diffusion to track the trajectories of electrons onto each pad. The results in Fig. 5 illustrate the final destination of each point charge after originating from the uniform discs of charge a few millimeters away. It is evident that despite the rather sharp points and edges of the zigzag structure, the collection of charge across the zigzag is quite uniform (at least for a 2-mm gap), thus making the zigzag a suitable structure for proportionally splitting charge, as hypothesized earlier. It should be noted that as part of the simulation, a ground plane was placed about 1/2 mm below the pad plane, sandwiching the FR4 substrate, which accounts for the fact that some charge is collected onto the gaps in between the pads. It is currently unclear exactly what effect the subsequent charging up of these gaps would have on the performance of the printed circuit board (PCB). Thus, in order to curb the potential nonlinearities, a guiding design principle is to maximize the area of the conductive layer by minimizing the gap spacing between pads.

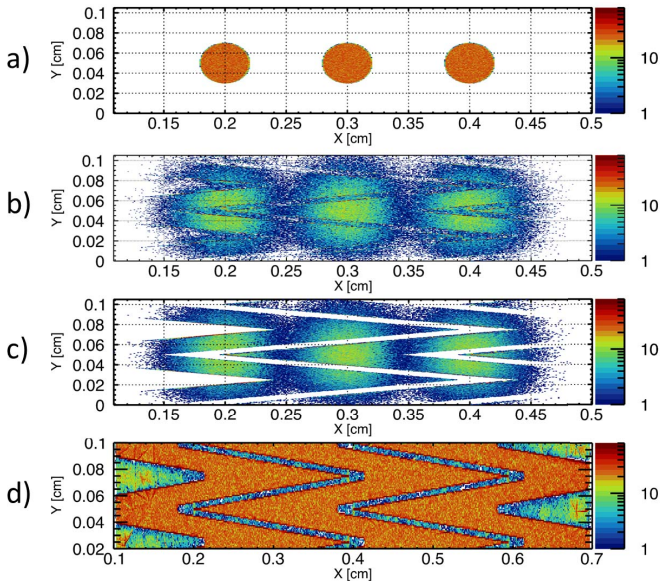

Fig. 5. (a) Three discs of uniformly distributed charge arranged on a plane 2 mm above the readout plane at the drift cathode. (b) Density of collected electrons onto the zigzag anode pad plane after drifting across the 2-mm gap and originating from the three discs. (The color scale is proportional to the charge density.) (c) Same plot as in (b) but with the electrons removed from the gaps to clearly reveal the zigzags, for reference. (d) Plane of uniform charge that fills the acceptance is collected onto the zigzag pads for the same detector configuration. In this case, the troughs of the zigzag were rounded to more accurately resemble actual manufactured electrodes.

B. Experimental Setup and Method

To verify the results from simulation, two readout PCBs with substantially different zigzag patterns were studied in the laboratory. Fig. 6 shows a detailed picture of the zigzag pattern for each PCB, at the same zoomed-in view level and scale. While the earlier PCB studied was designed conservatively to safely stay within the limits of manufacturability, the newer PCB design aimed at achieving a zigzag pattern as close to the ideal case described earlier. Specifically, the older PCB was fabricated by Accurate Circuit Engineering (ACE) [2],

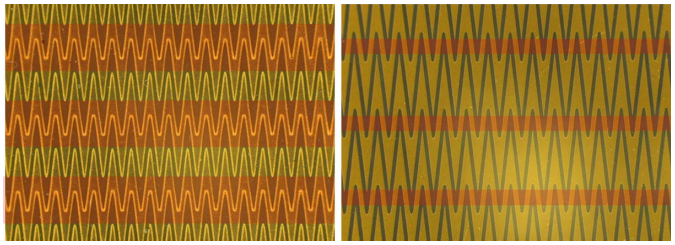

Fig. 6. Microscope photographs of the two zigzag PCBs studied (the same scale). PCB from an early zigzag design (made by ACE) (left) and PCB fabricated using the latest design (made by Somacis) (right). Table I tabulates the parameter specifications for each zigzag pattern. The red band in each photograph highlights the regions where there is no overlap between neighboring pads.

TABLE I

ZIGZAG PARAMETERS FOR THE ACE AND SOMACIS ZIGZAG DESIGNS, COMPARED TO THE MEASUREMENTS TAKEN WHILE INSPECTING THE ACTUAL PCBS

	Older PCB (ACE)		Newer PCB (Somacis)	
Zigzag parameter	Design	PCB	Design	PCB
pad pitch (mm)	2.000	2.000	2.000	2.000
zigzag period (mm)	0.500	0.500	0.587	0.587
gap width (mm)	0.078	0.082	0.075	0.084
trace width (mm)	0.175	0.159	0.155	0.141
pad overlap %	69	40	94	83
conductor coverage %	70	66	67	63

where the percentage pad overlap design parameter ended up being around 70%. This was essentially dictated by what could be made reliably using a standard etching process. The new design called for a pad overlap approaching 100% with the minimum gap width possible. The PCB had to be fabricated by pushing the limits of standard chemical etching techniques and was fabricated by Somacis, Inc. [9], who employed a specialized version of the standard process to generate the new PCB. Instead of making the percentage pad overlap exactly 100%, 94% was chosen since there must be a compromise with the degree of conductor coverage for a given gap width, which in this case was the minimal industry standard of 0.003" ($\sim$75 μm). While the parameters corresponding to the larger feature sizes of each design (pad pitch and zigzag period), were reproduced quite accurately by both manufacturers, the smaller features, including the trace and gap widths, were fabricated with far less accuracy, to within $\pm$5% of the design specifications. The design specifications and the measured physical dimensions of each PCB pattern are summarized in Table I.

Each PCB made up the readout plane of a quadruple GEM detector with a 10 cm $\times$ 10 cm active area consisting of 50 zigzag pads in 10-pad rows, each 10 mm long and extending almost 4 mm in the interleaving direction. Each pad is read out using a charge-sensitive preamplifier together with a shaping amplifier, and the analog waveform is digitized by a 100-MHz analog to digital converter. The detector chamber was purged with Ar/CO_2 70:30 for the working gas and operated at a gain of approximately 4.5×10^3 with a drift field of 0.75 kV/cm over a $\sim$1-cm drift gap, and 3 kV/cm applied

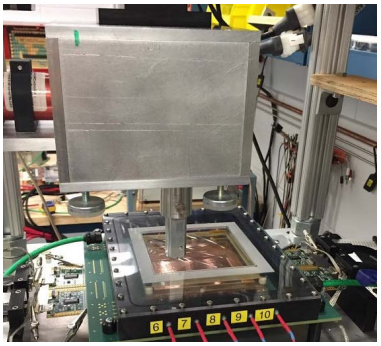

Fig. 7. Photograph of the experimental setup, showing the collimated X-ray source (aluminum box with protruding collimator), scanning the 10 cm $\times$ 10 cm Mylar window/acceptance of the quadruple GEM detector. The zigzag PCB can be seen at the bottom (green).

to the transfer and induction gaps. The detector was studied by illuminating the active area with a highly collimated beam of X-rays, with a cross section of roughly 100 μm $\times$ 8 mm. With the X-ray source mounted to a moveable *xy*-stage, the collimated beam was scanned across the active area of the detector in 100 μm steps, for a distance equal to several times the pad pitch along the position-sensitive coordinate. A photograph of the setup is shown in Fig. 7. After accounting for any misalignment in the setup, the resolution for the GEM detector was calculated at every step along the X-ray scan. The residual was taken as the difference between the calculated centroid (using the measured charge distribution) as defined in Fig. 1, and the actual hit position, taken to be the motor position of the X-ray source on the *xy*-stage, which has an uncertainty of less than 10 μm. The method by which the centroid was calculated used a charge threshold in an offline C++-based analysis to identify hits to form two-, three-, and four-pad clusters from which the centroid was derived.

While these in-laboratory measurements of resolution may be used to attach figures of merit to each zigzag pattern, these measurements are not fully representative of the true single-point track resolution. As such, the goal here was to maximize this relative measure of the resolution. It should also be noted that while the hit position used for the centroid is only known to within the width of the X-ray beam from the collimator, no attempt was made to unfold this width from the results since the beam profile is not accurately known. However, the width is estimated to be about 40–50 μm [13], which is a significant contributor to the quoted values of resolution and should in principle be reduced by this amount subtracted in the quadrature. Nevertheless, the quoted resolution from the X-ray scans are only considered relative metrics, so it is not imperative in this case to remove a constant term that is common to all measurements.

C. Measurement Results

Some of the detailed results from the Somacis PCB are shown in Figs. 8–10. The most remarkable characteristics of these measurements include a significant DNL and a nonuniform position resolution, as well as periodic cluster size variations along the readout. The centroid calculation excludes

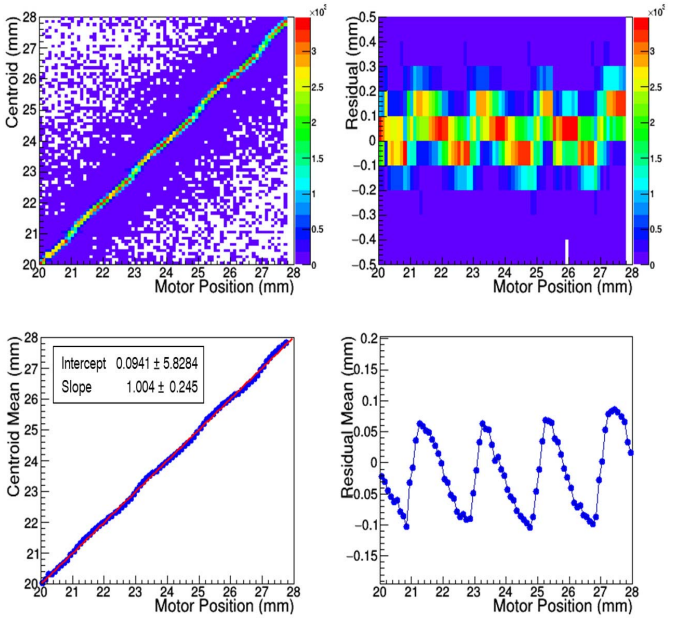

Fig. 8. Reconstructed hit position of each X-ray versus the motor position (top left) and corresponding residual versus motor position for the Somacis PCB (top right). Respective averages of these quantities, where the position correlation plot includes a red line with unity slope for reference (bottom).

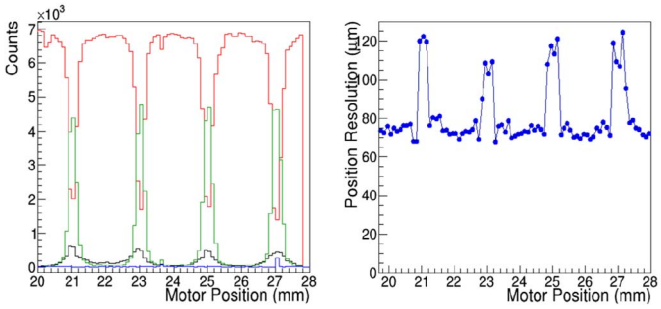

Fig. 9. Number of events with a given pad-cluster size and the resolution versus scan position, respectively, for the Somacis PCB. Black histogram corresponds to the number of events with single-pad clusters (left). Red: two-pad clusters. Green: three-pad clusters. Blue: four-pad clusters.

single-pad hits, so not all events are processed during the analysis. Fig. 10 (left) shows the resulting residual distribution corresponding to the full X-ray scan, while the second plot is the same distribution, but corrected for the observed DNL. Both are fit to a double Gaussian function to account for the magnitude of a nonnegligible background component found in each distribution. The DNL correction for the second plot involves removing the mean deviation from linearity for the centroid distributions at each point along the X-ray scan. The mean of the residual distribution for each position is purposefully centered on zero, which removes the DNL before the histogram entries are added to the cumulative residual plot. In contrast, the first plot is a simple aggregate of all the raw position residual distributions, which retain the mean deviation. The mean of the residual distribution at each point along the scan is plotted against the X-ray position in Fig. 8 (bottom right), which directly shows the offsets applied for the DNL correction.

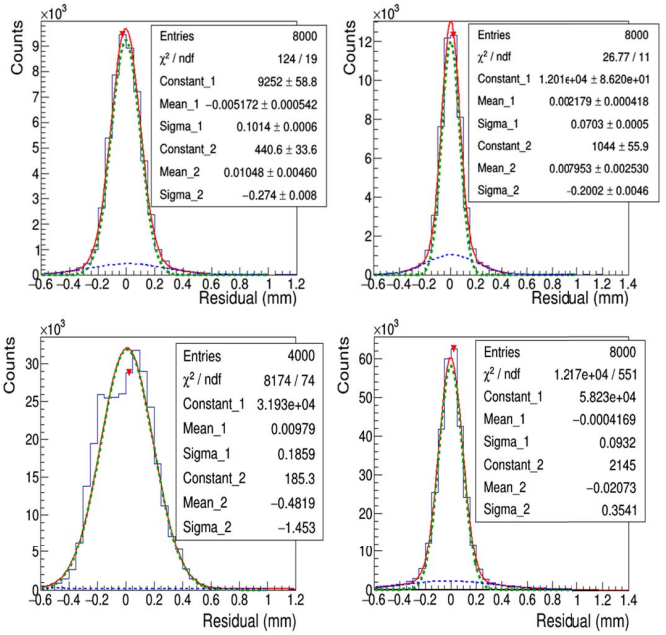

Fig. 10. Position residual distribution integrated over ∼four pitch cycles, without and with the DNL correction, respectively, for the Somacis PCB (top) and ACE PCB (bottom). The components of a double Gaussian fit to the distributions are drawn as green and blue dashed lines for the dominant and background components, respectively, while the sum of these components is drawn as a red solid line. "_1" and "_2" identify the dominant and background Gaussian component parameters, respectively.

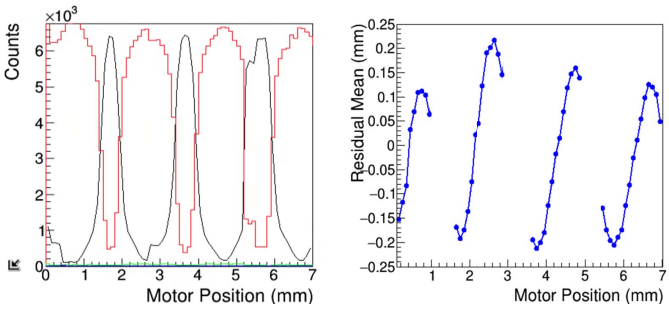

Fig. 11. Number of events with a given pad-cluster size and the mean position residual versus scan position, respectively, for the ACE PCB.

The pertinent results for the ACE PCB are shown in Figs. 10 and 11. The most notable differences in these results include a large increase in single-pad hits for the ACE PCB and the suppression of three-pad events. At the same time, the residual distributions for the ACE PCB show smaller background components; the background component for the Somacis PCB accounts for 13% of all events (with no DNL correction applied) and 22% (with the DNL correction), while the same quantities are 4% and 12%, respectively, for the ACE PCB.

The plots in Fig. 12 show the relative response of each pad as they are irradiated during the X-ray scan (adjusted to remove the influence from variations in the detector gain). The amount by which the curves overlap indicates that the pad pitch is generally appropriate for the size of the charge cloud, although the increased overlap of the curves for the Somacis

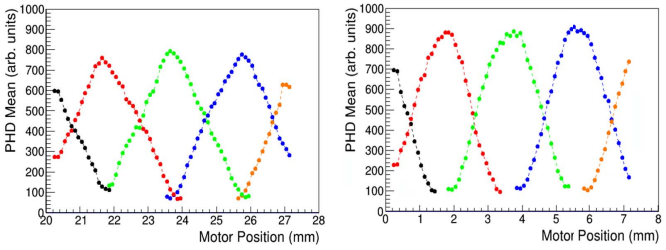

Fig. 12. Mean of pulse height distributions for each pad versus X-ray source position on readout plane for both the Somacis and ACE PCB, respectively. Each colored curve corresponds to the signal response from five different sequential pads.

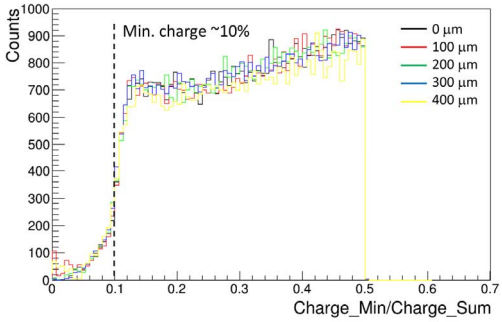

Fig. 13. Spectra of the minimum-charge-to-total-charge ratio for two-pad hits for five distinct points along the zigzag period in 100-μm steps for the Somacis PCB. In this case, the collimator slit width spans four to five pads, so these results show the charge ratio integrated over several pads.

PCB at lower signal amplitudes demonstrates superior charge sharing. In addition, the curves for the ACE board exhibit somewhat flatter peaks, which also suggest a suppressed sensitivity to the position of the moving source.

Finally, as shown in Fig. 13, a scan perpendicular to the sensitive coordinate (with the 8-mm length of the collimator slit now parallel to the sensitive coordinate and spanning four to five pads) was performed for the Somacis PCB to measure the full charge ratio spectrum for two-pad hit events, which comprise the vast majority of all events. While the charge-sharing profile is quite consistent everywhere along the zigzag period as expected, there is also a sharp cutoff at around 10%. This implies that the minimal charge any one pad collects is most often above 10%, which is a critical feature when considering practical issues such as the S/N ratio of the front-end electronics.

D. Discussion

Overall, the results from the Somacis PCB show markedly improved performance compared to the ACE PCB. The ACE PCB is outfitted with zigzag pads with the same pitch and a similar zigzag period, gap width, and conductor coverage as the Somacis PCB but with significantly less pad overlap. Although all but one of the physical properties of the two boards are comparable, X-ray scans performed with the ACE PCB under similar conditions resulted in an integrated position resolution of 186 and 93 μm with and without applying a DNL correction, respectively (taken as the width of the dominant

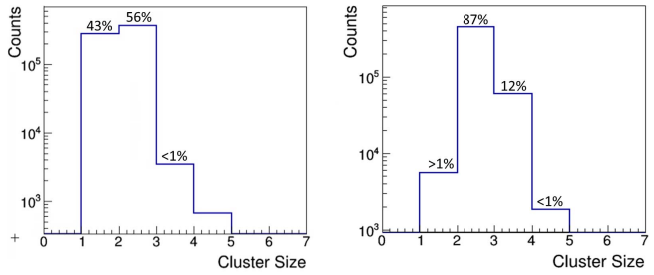

Fig. 14. Cluster size distributions for the ACE and Somacis PCB, respectively.

Gaussian components in Fig. 11), compared to 101 and 70 μm for the Somacis board (shown in Fig. 10). It must be noted that the background components do not contribute to the quoted resolutions, but represent some fraction of the detector response with substantially worse resolution. While the Somacis PCB is described as having superior resolution, its background is notably higher than in the case of the ACE PCB.

Despite having larger backgrounds, the maximum mean excursion from linearity was only $\sim$75 μm for the Somacis PCB, but was about twice this value for the ACE board [as indicated in Fig. 8 (bottom right) and Fig 11 (right)]. In addition, single-pad hit events were pervasive for the ACE PCB as seen from Fig. 11 (left) compared to the similar plot in Fig. 9 for the Somacis board. In particular, there is a clear shift in the cluster size distribution for these two PCBs, as shown in Fig. 14, where the single-pad hit events dropped from about 43% of all events for the ACE PCB to only a little over 1% for the Somacis board. We believe that these considerable performance improvements are the result of the improved linearity in charge sharing due to the significantly greater percent overlap of neighboring pads in the Somacis board.

The improved detector performance of the Somacis PCB is very encouraging, which mostly validates the conclusions drawn from simulation. However, the results obtained thus far are still far from ideal, mainly due to the prevalence of a notable DNL, in addition to spikes in the position resolution and the long tails observed in the residual distributions of both PCBs.

By examining Fig. 15, it is clear that systematic global shifts in the reconstructed position (i.e., the observed DNL) for the ACE PCB are an unavoidable consequence of nonideal zigzag geometries. In Fig. 15, the greatest excursions from linearity coincide with areas on the readout with no pad overlap (red bands) and consequently poor charge sharing. Points on the curve showing the smallest deviation correspond to the overlap region (near the blue dashed line) with optimal charge sharing, as expected. Fig. 16 conceptually illustrates how this systematic shift of the centroid is manifested: starting with the ideal zigzag geometry, areas near the pad centers are designated as regions absent of charge sharing (outlined by the red vertical bands), which in principle represent sites in actual PCBs where there is no pad overlap. The consequence of this distorted zigzag geometry is that a portion of the

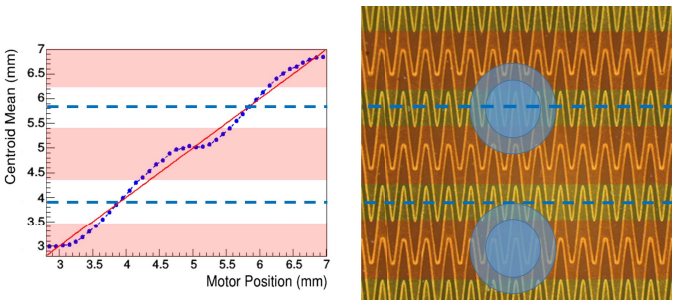

Fig. 15. Zoomed-in view plot of the actual X-ray position versus the reconstructed position using measurements taken with the ACE PCB. The horizontal red bands correspond to areas near pad centers as shown on the zoomed-in view picture of the readout to the right. The dashed blue line corresponds to the midway point between the pads. Diagonal red line: perfect linearity for comparison (left). Blue circles: charge clouds collected by neighboring pads.

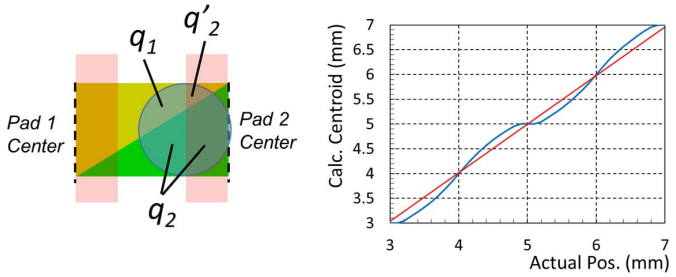

Fig. 16. Sketch of ideal zigzag pattern distorted by designating areas at the pad center (using red vertical bands) regions where charge sharing is absent. q_1, q_2, and q_2' represent portions of the charge cloud collected by the two pads. The plot is the results of a simple arithmetical model of this charge-sharing scheme (left).

charge that would normally be collected by one pad is diverted and collected by its neighbor, thus skewing the centroid from linearity. The degree of skewing depends on the magnitude of the diverted charge, which is clearly exacerbated if the region in red were larger. In the extreme case, the plateau regions near pad centers in the position correlation plot correspond to single-pad events where there is zero charge sharing, resulting in virtually no positional sensitivity between the pads. At the midway point between two pads, charge sharing is symmetric, resulting in zero DNL. In the ideal case, the expression for the centroid would be

$$X = ((q_1 + q_2')x_1 + q_2 x_2)/Q$$

whereas in the realistic case, the expression takes on this form:

$$X = (q_1 x_1 + (q_2 + q_2')x_2)/Q$$

where Q is the total sum charge collected by all pads and q_2' is the magnitude of the diverted charge. A simple mathematical model demonstrates the behavior of the centroid if such diverted charge sharing is present in the system. The results of this model nicely reproduce the observed response of the ACE PCB readout and are shown in Fig. 16.

Another implication of irregular charge sharing along the zigzag structure is the formation of long tails in the position residual distributions for both PCBs. As shown in Fig. 17, the residual distributions at certain points along the X-ray scan

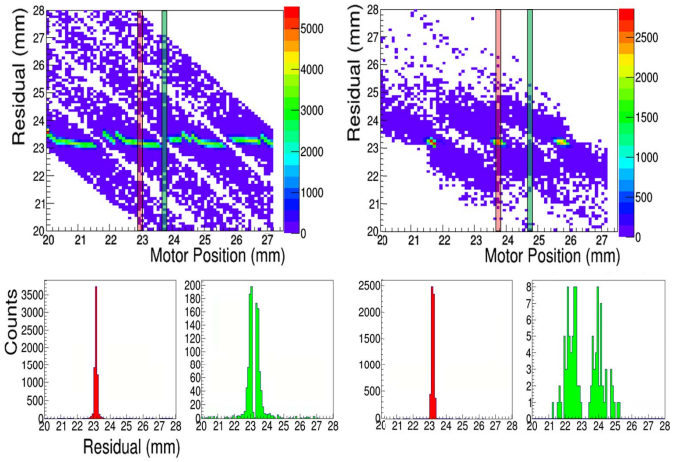

Fig. 17. Position residual versus X-ray source position for two- and three-pad cluster events, respectively, for the Somacis PCB are shown in scatter plots (top). The two histograms beneath each scatter plot represent residual distributions at two specific locations along the zigzag; the red histograms correspond to the pad centers, denoted by the red vertical bands in each scatter plot and the green histograms correspond to the areas between pads, denoted by the green bands.

can vary quite significantly from the norm. The most notable areas are not surprisingly the middle of each pad, where charge sharing tends to break down. In the case of purely two-pad clusters, the prevalent diagonal valleys of empty events in the left scatter plot create gaps in the residual distribution. At the pad center, the result is a broad, double-peaked distribution, which mostly accounts for the long tails in the cumulative residual plot. The double peak is due to clusters made up of two different pairs of pads; at the pad center, the smaller charge collected by a pad can either fall to the left or right of the central pad, giving rise to a disjoint centroid distribution.

For the Somacis PCB, three-pad events exhibit double peaking in between the pads, with narrow distributions at the centers. Thus, three-pad clusters allow the Somacis PCB to maintain sensitivity at the pad centers, while the considerably fewer two-pad events here simply contribute to background. In the case of the ACE PCB, the three-pad events are almost nonexistent and have given way to a significant number of single-pad hits which create dead zones near the pad centers with virtually no positional sensitivity. In addition, the two-pad cluster events that are prominent for the Somacis PCB at the pad centers are missing for the ACE PCB, which tends to minimize the background component of the cumulative residual distribution for the ACE PCB.

We have shown that the observed nonuniformities in position resolution, the DNL, and the background position residuals measured for two different zigzag pad readouts are all due biases in the division of charge in nonideal zigzag patterns. We have also shown via simulation that these biases are mostly absent in idealized zigzag geometries. It is therefore reasonable to expect that the observed undesired behavior would be mitigated for PCBs with zigzag patterns closely resembling the ideal one. Consequently, the focus of our future research and development program is shifted toward finding ways to realize a zigzag structure as close to the ideal pattern as possible. In particular, the next critical step

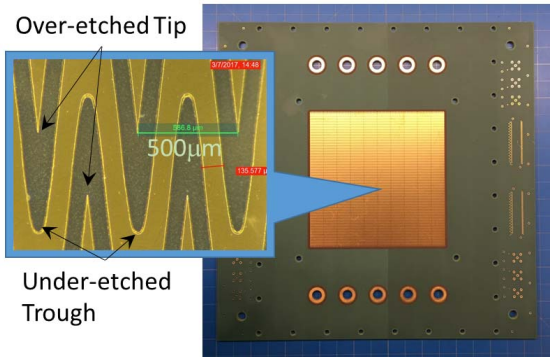

Fig. 18. Zoomed-in view features of the zigzag pattern from the Somacis PCB produced using standard chemical etching. The tips have been eroded by more than 125 μm and the troughs undercut by 200–300 μm.

is to overcome the distortions imposed by the fabrication process. Fig. 18 shows the two predominant distortions of the zigzag geometry resulting from standard chemical etching, including overetching of the zigzag tips as well as under-etching at the troughs. These distortions put an upper limit on the pad overlap specification and contribute to deviations from the ideal pattern. Hence, together with the limitations on the minimum gap width, the potential for implementing an optimally linear charge-sharing model in a working detector is severely hampered by this manufacturing technique.

As a next phase of the research and development program, we are thus pursuing new fabrication processes that do not suffer from the limitations described earlier. In particular, the novel use of laser ablation using ultrashort and focused pulses of light to remove copper from the PCB substrate is well suited for accurately reproducing the fine detail of the zigzag structure. Such advances in the printed circuit industry will then allow one to probe regions of the zigzag geometry parameter space down to the level of .001" ($\sim$25 μm) or less. For example, the 83% pad overlap and 63% conductor coverage of the Somacis PCB may be pushed to exactly 100% overlap and 92% conductor coverage if a minimal gap width of just below .001" can be achieved, free of the mentioned geometric distortions. Based on the significant improvements already seen between the ACE and Somacis PCB designs, a substantial improvement in performance can therefore be expected for a PCB produced using laser ablation.

It should be noted that there have also been preliminary attempts to compensate for the manufacturing distortions described earlier by implementing design features such as overstretched zigzags [13]. However, such techniques have had limited success, likely because identifying the optimal compensating design requires a dedicated effort beyond what was initially tried.

III. Conclusion

With guidance from simulation, we have come closer to optimizing the design of a GEM readout using zigzag patterns. Two prototype PCBs consisting of two variants of the zigzag pattern were produced and tested on the bench using collimated X-rays and showed a position resolution at around 100 μm using a relatively coarse segmentation, with a pitch roughly the size of the impingent charge cloud. In the process, we have also identified major limitations for the fabrication of the zigzag pads, which severely limits the potential performance of the ideal pad designs. However, we believe that by overcoming such limitations, the use of zigzag pads can be broadly implemented as an alternative to many highly segmented, and therefore very costly readout options.

References

[1] D. Abbaneo, "Beam test results of new full-scale prototypes for CMS high-eta muon system future upgrade," in *Proc. IEEE Nucl. Sci. Symp. Conf. Rec.*, Oct./Nov. 2012, pp. 1172–1176.

[2] *Printed Circuit Board Manufacturer*, Accurate Circuit Eng., Inc, Santa Ana, CA, USA, 2014.

[3] B. Azmoun *et al.*, "A study of a mini-drift GEM tracking detector," *IEEE Trans. Nucl. Sci.*, vol. 63, no. 3, pp. 1768–1776, Jun. 2016.

[4] J. Barrette *et al.*, "A study of MWPC with chevron cathode pad readout," *Nucl. Instrum. Methods Phys. Res. A, Accel. Spectrom. Detect. Assoc. Equip.*, vol. 385, no. 3, pp. 523–529, 1997.

[5] Y. Giomataris, P. Rebourgeard, J. P. Robert, and G. Charpak, "MICROMEGAS: A high-granularity position-sensitive gaseous detector for high particle-flux environments," *Nucl. Instrum. Methods Phys. Res. A, Accel. Spectrom. Detect. Assoc. Equip.*, vol. 376, no. 1, pp. 29–35, 1996.

[6] J. Kaminski, S. Kappler, B. Ledermann, T. Muller, and M. Ronan, "Study of various anode pad readout geometries in a GEM-TPC," *IEEE Trans. Nucl. Sci.*, vol. 52, no. 6, pp. 2900–2906, Dec. 2005.

[7] T. Miki, R. Itoh, and T. Kamae, "Zigzag-shaped pads for cathode readout of a time projection chamber," *Nucl. Instrum. Methods Phys. Res. A, Accel. Spectrom. Detect. Assoc. Equip.*, vol. 36, no. 1, pp. 64–68, 1985.

[8] F. Sauli, "GEM: A new concept for electron amplification in gas detectors," *Nucl. Instrum. Methods Phys. Res. A, Accel. Spectrom. Detect. Assoc. Equip.*, vol. 386, nos. 2–3, pp. 531–534, 1997.

[9] *Printed Circuit Board Manufacturer*, Somacis, Inc., Poway, CA, USA, 2017.

[10] The sPHENIX collaboration. (Feb. 27, 2018). *sPHENIX Conceptual Design Report*. [Online]. Available: https://indico.bnl.gov/event/4315/attachments/11945/14626/sphenix-conceptual-design.pdf

[11] B. Yu *et al.*, "A GEM based TPC for the LEGS experiment," in *Proc. IEEE Nucl. Sci. Symp. Conf. Rec.*, vol. 2, Oct. 2005, pp. 924–928.

[12] B. Yu, V. Radeka, G. C. Smith, C. L. Woody, and N. N. Smirnoff, "Study of GEM characteristics for application in a MicroTPC," *IEEE Trans. Nucl. Sci.*, vol. 50, no. 4, pp. 836–841, Aug. 2003.

[13] A. Zhang, M. Hohlmann, B. Azmoun, M. L. Purschke, and C. Woody, "A GEM readout with radial zigzag strips and linear charge-sharing response," *Nucl. Instrum. Methods Phys. Res. A, Accel. Spectrom. Detect. Assoc. Equip.*, vol. 887, pp. 184–192, Apr. 2018.

[14] A. Zhang, "Performance of a large-area GEM detector read out with wide radial zigzag strips," *Nucl. Instrum. Methods Phys. Res. A, Accel. Spectrom. Detect. Assoc. Equip.*, vol. 811, pp. 30–41, Mar. 2016.